PHYSICAL REVIEW D **90,** 054023 (2014)

Polarized WW scattering on the Higgs pole

Johann Brehmer, Joerg Jaeckel, and Tilman Plehn

Institut für Theoretische Physik, Universität Heidelberg, Philosophenweg 16, 69120 Heidelberg, Germany

(Received 4 July 2014; published 23 September 2014)

The Higgs discovery has given us the Higgs–gauge sector as a new handle to search for physics beyond the standard model. This includes physics scenarios originally linked to massive gauge boson scattering at high energies. We investigate how one can separately probe the Higgs couplings to the longitudinal and transverse parts of the massive gauge bosons away from this high-energy limit. Deviations from the standard model could originate from higher-dimensional operators, compositeness, or even more fundamentally from a violation of gauge invariance. The signature we propose is the tagging jet kinematics in weak boson scattering for scattering energies close to the Higgs resonance. During the upcoming LHC run at 13 TeV we will be able to test these couplings at the 20% level.

DOI: 10.1103/PhysRevD.90.054023 PACS numbers: 13.88.+e, 12.60.Fr, 14.80.Bn

I. INTRODUCTION

With the discovery of a scalar Higgs boson [1,2] the standard model of particle physics is finally complete. However, many experimental and theoretical questions are left unanswered [3]: not least among them is the question about the smallness of the Higgs mass, or more precisely the electroweak scale, when compared to the Planck scale. Are the interactions of the most fundamental particles really described by perturbative field theories all the way to the Planck scale [4]? Also the symmetry structure of the SM itself is surprising; why do we observe an $\mathrm{SU}(3) \times \mathrm{SU}(2) \times \mathrm{U}(1)$ gauge symmetry?

One way to make progress on these questions is theoretical model building. At the same time, however, it is crucial that we check the underlying assumptions of the standard model by experimentally testing the predictions following from its basic structure. In that one should leave no stone unturned, including tests of the nature of gauge invariance itself.

The discovery of the Higgs opens exciting new possibilities to test the standard model, in particular with the above questions in mind. The scalar nature of the Higgs is responsible for the hierarchy problem, and indeed the Higgs is the only scalar which could be a fundamental noncomposite particle. At the same time the Higgs mechanism is responsible for generating the masses of the W and Z bosons and is therefore intimately linked to the $\mathrm{SU}(2) \times \mathrm{U}(1)$ gauge structure. The Higgs–gauge sector therefore provides an ideal laboratory to probe both the hierarchy problem and the gauge structure of the standard model. Specifically, measurements of Higgs couplings to vector bosons as probed in VV scattering processes ($V = W, Z$) are ideal for this endeavor.

Historically, the question used to be how VV scattering is unitarized or how its amplitude behaves at high energies. The corresponding experimental signature is VV scattering at high energies, described by the Goldstone equivalence theorem. By now we know that the observed Higgs boson will at least significantly dampen the ultraviolet behavior of VV scattering [5]. The questions

(i) How does the VV scattering amplitude behave at high energies?
(ii) Does the observed Higgs boson render VV scattering weakly interacting?
(iii) Does the HVV interaction correspond to the standard model prediction?

are equivalent in their theoretical implications, even though they seem to require very different experimental strategies. In this paper we propose to follow the third question, because there exists plenty of experimental data from Higgs analyses which allows us to test the structure of the HVV vertex to gain insight into the underlying fundamental physics.

The Higgs–gauge sector is often approached using an effective field theory approach in terms of higher-dimensional operators. While it follows naturally from the observation that gauge field theories describe the fundamental interactions of particles [6], the greatest advantage of this approach is its greatest shortcoming: it usually assumes (part of) the symmetry structure of the standard model and hence makes it harder to study the fundamental symmetries underlying the standard model.

In this paper we are a bit more heretical: we propose to *separately* test the Higgs couplings to transverse and longitudinal parts of the massive gauge bosons. This is inspired by the approximate notion that the transverse parts correspond to the "proper" gauge bosons, whereas the longitudinal parts arise from the eaten Goldstone bosons. A clean separation is only possible at infinitely large momenta or in the nearly massless limit [7], at which we cannot operate when interpreting LHC Higgs data. However, this technical problem does not render the physics question of coupling massive gauge bosons with different polarizations to the Higgs boson any less relevant. Indeed, through the explicit definition of polarization in a

simple model we have to break Lorentz invariance. Nevertheless, we view it as a first step toward individually testing the physics of the Higgs and its Goldstone bosons and that of the original non-Higgsed gauge bosons.

On the theory side, composite Higgs bosons are studied in great numbers and detail. However, much less attention has been paid to the known possibility that the gauge bosons can be composite particles of an emergent gauge symmetry [8]. As an example, vector meson dominance in QCD can be viewed as an (approximate) emergent gauge symmetry [9]. Moreover, supersymmetric theories often have completely different gauge symmetries in the infrared and in the ultraviolet, as made explicit by the Seiberg duality [10]. The gauge symmetry can be larger in the infrared than in the ultraviolet regime and therefore does not simply correspond to a Higgsed case. Indeed, the new degrees of freedom can be viewed as solitons of the original theory and are nontrivial in this sense. In this paper we take the first steps to develop tools to experimentally distinguish between a composite Higgs sector and composite gauge bosons. The question to how well our question and our findings can be described in terms of higher-dimensional operators will be discussed at the end of the paper.

Our laboratory to probe the structure of the HVV interaction is VV scattering as depicted in Fig. 1. At large energies this process has been discussed extensively [11]. For example in the Refs. [12] the authors develop analysis strategies to select highly energetic longitudinal gauge bosons in all leptonic VV topologies, including jet tagging, a central jet veto, and back-to-back lepton geometries. In Ref. [13] semileptonic W^+W^- decays are first analyzed based on boosted W tagging. The full set of semileptonic VV channels is discussed in Ref. [14]. As pointed out in Ref. [15] these high-energy VV signatures suffer not only from low rates, but also from large scale uncertainties. The measurement of the relative longitudinal and transverse polarizations based on decay angles can be used to avoid large QCD uncertainties on LHC rates.

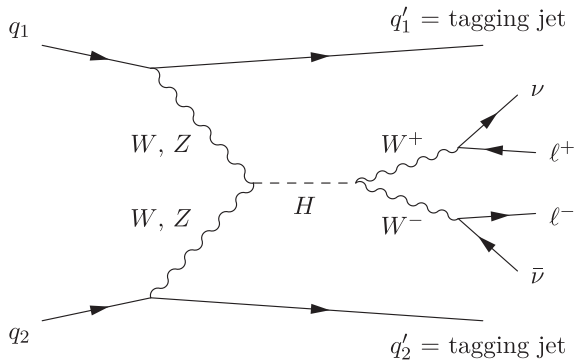

FIG. 1. VV scattering process we consider in this paper, $V = W$. Our analysis shows that indeed the Higgs resonance region is where we can best test the Higgs–gauge structure in and beyond the standard model.

In contrast to all this earlier work our main focus lies on weak–boson–fusion production of massive gauge bosons close to the Higgs resonance, which enhances the event rates. Instead of using the high-energy behavior of the vector bosons, we look at the tagging jets and in particular their high-energy behavior. Beyond the interpretation in specific models our analysis therefore develops a set of new observables that are sensitive to the structure of the Higgs–gauge sector.

The paper is structured as follows: in Sec. II we start with our definition of transverse and longitudinal gauge bosons. Then, in Sec. III we develop our analysis strategy and contrast it with the established studies of the high-energy regime and the Higgs decay correlations. The results of our tagging jet analysis follow in Sec. IV. Section V is devoted to a discussion of the frame dependence of polarizations. Finally, in Sec. VI we relate our findings to the usual effective field theory approach based on higher-dimensional Higgs–gauge operators.

II. A SIMPLE MODEL

Even in the absence of an immediate field theoretical description, the polarization of massive spin-1 gauge bosons coupling to the Higgs bosons is a property of the W and Z bosons worth testing at the LHC. As alluded to in the Introduction, the coupling of the Higgs boson to transverse and longitudinal gauge bosons has a very different origin. This aspect is obvious when we go into the high-energy limit, where the longitudinal degrees of freedom correspond to the Goldstone modes of a Higgs sigma field and where the transverse polarization modes are suppressed by powers of M_V/E. At finite energies and for example in unitary gauge we have to define and separate the transverse and longitudinal degrees of freedom by hand.

In spite of this complication, measuring the polarization of the gauge bosons coupling to the Higgs will allow us to test the underlying structure of electroweak symmetry breaking. The HVV couplings ($V = W, Z$) mediating both, Higgs production in weak boson fusion and Higgs decays to leptons, require us to define the polarization of the gauge bosons for off-shell and on-shell states. We define the transverse and longitudinal parts of the W- or Z-boson fields as

$$V_T^\mu = \mathbb{P}^\mu_\nu V^\nu \quad \text{and} \quad V_L^\mu = (\mathbb{1} - \mathbb{P})^\mu_\nu V^\nu, \tag{1}$$

in terms of the W, Z boson in unitary gauge and the projection operator $\mathbb{P}^{\mu\nu}$

$$\mathbb{P}^{0\nu} = 0 = \mathbb{P}^{\mu 0} \quad \text{and} \quad \mathbb{P}^{ij} = \delta^{ij} - \frac{\vec{p}^{\,i}\vec{p}^{\,j}}{\vec{p}^{\,2}} \quad (i, j = 1, 2, 3). \tag{2}$$

This allows us to split the Higgs–gauge vertex into its polarization components. Measuring polarizations requires

a specific reference frame. We choose to evaluate Eq. (1) in the Higgs rest frame. This definition, which we will justify below, gets rid of mixed couplings HV_LV_T in the Higgs–gauge coupling structure $HV_LV_L + HV_TV_T$. The remaining two contributions to the HVV coupling can be written in terms of the standard-model coupling strength $g_{\rm SM}$ and two scaling parameters

$$\mathcal{L} \supset -g_{\rm SM} H (a_L V_{L\mu} V_L^{\mu} + a_T V_{T\mu} V_T^{\mu}). \tag{3}$$

The sign of the real scaling parameters a_L and a_T is free, and we do not enforce a sum rule to protect the total Higgs production and decay rates.

As already mentioned, this simple model in terms of transverse and longitudinal polarizations requires a choice of reference frame and therefore breaks Lorentz invariance. Our simple model is also clearly not gauge-invariant. However, independent longitudinal and transverse Higgs–gauge couplings can be induced by perfectly valid models respecting the symmetries of the standard model. We will demonstrate this in Sec. VI, where we link our simple model to higher-dimensional operators. In this effective field theory approach, the couplings a_L and a_T become momentum-dependent. The correspondence to our simple model is most obvious if we define polarizations in the Higgs rest frame, justifying the choice made above. Alternative definitions will be discussed in Sec. V.

Regardless of these complications, the simple model exhibits a straightforward correspondence to the appropriate definition of longitudinal and transverse gauge bosons in the high-energy limit, which is precisely what we want to probe. We will therefore use it as a test scenario for our LHC analysis.

III. TAGGING JET KINEMATICS

Higgs production in weak boson fusion probes the HVV coupling structure in the initial state. Similarly, the VV decays test the same coupling in the final state. Due to the dependence on the initial state couplings the energy scales probed by the initial vertex are not automatically limited to the Higgs mass, as is the case for Higgs decays. Without any requirements on the intermediate Higgs state, the relevant process is W pair production in weak boson fusion at the perturbative order $\mathcal{O}(\alpha^4)$,

$$pp \to W^+W^- jj \to (\ell^+\bar{\nu})(\ell^-\nu) jj. \tag{4}$$

The on–shell Higgs diagram contributing to this process is shown in Fig. 1. Because the observed Higgs boson has essentially standard-model–strength couplings to the weak gauge bosons, we know that a large fraction of the rate for the full process in Eq. (4) comes through the s-channel Higgs resonance. In that case one of the two W bosons will be far off its mass shell and the Higgs resonance can be extracted with a transverse mass variable. This channel is maximally sensitive to the HWW coupling structure, which governs both the Higgs production and decay.

We generate event samples for the process given in Eq. (4) assuming an LHC energy of 13 TeV with MadGraph5 [16] using an in-house implementation of the model described in Sec. II. Because it is clear that the weak–boson–fusion features can be experimentally extracted [17], we limit ourselves to the parton level and omit systematic uncertainties in this first study. For the Higgs signal we assume a Higgs mass of 125 GeV and a Higgs width of 4.4 MeV, calculated with HDecay [18]. The polarizations of the W and Z bosons are defined according to Eq. (1).

Before we start with our tagging jet analysis we need to briefly motivate two choices which we make in analyzing the signal process given in Eq. (4), namely that we

(1) focus on the Higgs pole rather than on the high-energy regime, and
(2) analyze the tagging jets in addition to decay correlations.

The analysis of the process given in Eq. (4) in the search for nonstandard strong interactions in the gauge sector has a long tradition [12,13]. The main observable in such analyses is the invariant mass of the WW system or any approximation to it. In the high-energy limit this process should follow the equivalence theorem [7] and be dominated by the Goldstone modes of the massive W bosons. This is exactly the behavior we see in the left panel of Fig. 2, where we simulate events for weak–boson–fusion W pair production. In the setup where the Higgs couples only to transverse gauge bosons we observe a significant rate enhancement for $m_{WW} \gtrsim 1$ TeV. This is due to the missing cancellation with the scattering of longitudinal gauge bosons mediated by a Higgs exchange. In contrast, a Higgs coupling only to longitudinal gauge bosons is indistinguishable from the standard model case, showing that little cancellation is at work. In the same distribution we can also see the main problem with such an analysis: the fraction of events populating the phase space regions sensitive to modified Higgs–gauge couplings is depressingly small.

Moreover, after the Higgs discovery the motivation for this kind of challenging analysis is less straightforward. First, we can assume that the ultraviolet behavior of WW scattering is at least to a large part cured by the observed Higgs boson. This postpones any nontrivial behavior to much higher energies and therefore lower cross sections. Second, we can measure the Higgs properties, like the structure of the HVV vertex and its coupling strength, and based on those results reliably predict the behavior of the WW scattering at high energies. Given that most of the rate for $qqWW$ production comes from the Higgs pole region it is natural to replace the analysis of strongly interacting WW scattering by a dedicated study of $qqWW$ production around the Higgs pole. An explicit study of the actual

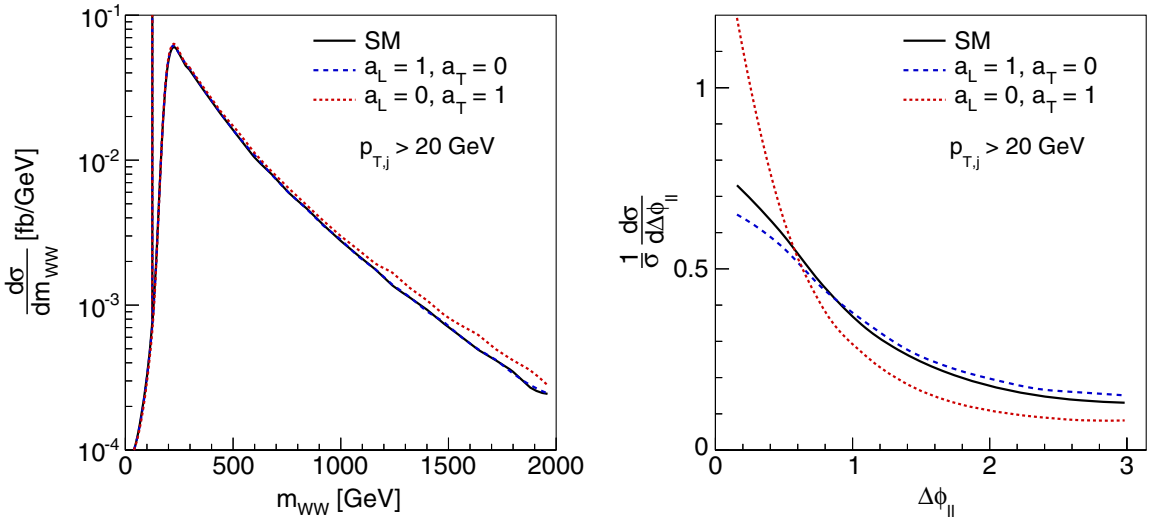

FIG. 2 (color online). Left: m_{WW} distribution for the signal process defined in Eq. (4) for a Higgs coupling exclusively to transverse or longitudinal gauge bosons as well as the standard model case. Right: $\Delta\phi_{\ell\ell}$ distributions of the Higgs decay leptons for the same three setups. We require $p_{T,j} > 20$ GeV to remove photon exchange contributions.

WW scattering process is of course still welcome and interesting, but would require a different interpretation.

The second choice is less obvious. Clearly, the Higgs decay leptons and the missing transverse momentum provide a handle to the final WW system. As a matter of fact, the LHC analyses leading to the Higgs discovery [2] already use a correlation between the two leptons reflecting the scalar nature of the intermediate resonance [19]. The most straightforward observables related to polarizations are decay angles [15]. In the presence of two neutrinos alternative observables include the lepton transverse momenta, the dilepton mass $m_{\ell\ell}$, the azimuthal angle between the leptons $\Delta\phi_{\ell\ell}$, and the missing transverse momentum p_T^{miss}. For illustration purposes we show the $\Delta\phi_{\ell\ell}$ distribution for the process $qq \to qqH \to qq(W^+W^-)$ in the right panel of Fig. 2. Unlike for the m_{WW} distribution the distinguishing features now reside in a phase space region with a significant number of events. The main question in this case becomes how much of this difference survives acceptance cuts, background rejection cuts, and detector effects [15].

Instead of the Higgs decay products we will focus on the tagging jets. Their kinematic distributions are sensitive to the initial HVV vertex structure [20,21] and the polarization of the fusing gauge bosons. While originally developed for weak boson fusion, the same features can be used for example in Higgs production [22,23] or in top pair production in gluon fusion [24]. In the following we will see that this tagging jet information includes the same kind of information on the gauge boson polarization as the Higgs decay correlation. However because it is independent of the Higgs decay channel, it can be measured in many different signatures, allowing for an efficient test of the results from individual Higgs decay channels.

We can analytically formulate the relation between polarization of the weak bosons and the transverse momenta of the tagging jets in the effective W approximation (EWA) [25]. It treats the initial gauge bosons as on-shell propagators and factorizes the weak–boson–fusion process into the radiation of a collinear W off a quark and the hard scattering process of the two W bosons. Similar to a p_T-dependent leading-order QCD parton density we can define a probability of finding a W boson radiated off the incoming quark with a longitudinal momentum fraction x and the transverse momentum p_T. For the respective polarizations they read

$$P_T(x,p_T) = \frac{g^2}{16\pi^2}\frac{1+(1-x)^2}{x}\frac{p_T^3}{((1-x)m_W^2+p_T^2)^2}$$
$$P_L(x,p_T) = \frac{g^2}{16\pi^2}\frac{1-x}{x}\frac{2(1-x)m_W^2 p_T}{((1-x)m_W^2+p_T^2)^2}. \quad (5)$$

The two distributions have a different p_T dependency: tagging jets recoiling against a longitudinal W should be softer than those recoiling against a transverse W.

The theoretical predictions shown in Eq. (5) are a promising basis to test the longitudinal vs transverse structure of the HVV coupling in weak boson fusion. However, we first need to see if the assumptions underlying the effective W approximation actually hold. To consider the W to be essentially a parton inside the proton there needs to be a hierarchy $E_{\text{proton}} \gg m_{\text{hard}} \gg m_W$. In our case the hard process is the $2 \to 2$ scattering $W^+W^- \to W^+W^-$, where the two relevant Mandelstam variables scale like $|t| < s = m_{\text{hard}}^2$. For the full $2 \to 4$ process the additional two energy scales defined by the tagging jet momenta then have to be $p_{L,j} \gg m_{\text{hard}} \gg p_{T,j} \sim m_W$ [26–28].

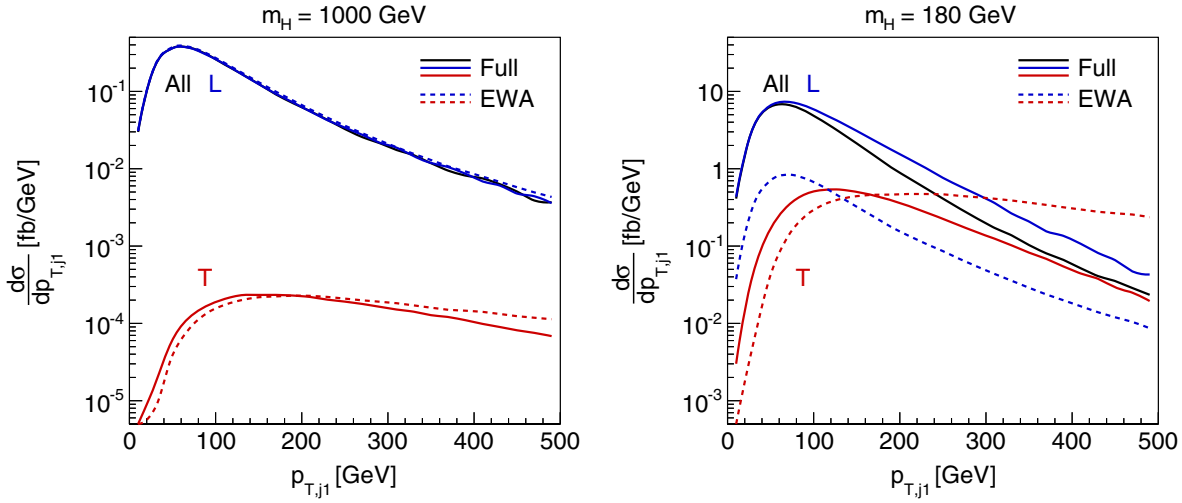

FIG. 3 (color online). Normalized $p_{T,j1}$ distributions for the complete signal process defined in Eq. (4) and in the effective W approximation, assuming a heavy Higgs with $m_H = 1$ TeV (left) and $m_H = 180$ GeV (right).

The physical Higgs mass of $m_H = 125$ GeV is too close to the W mass and the conditions for the validity of the EWA are not fulfilled. We nevertheless find that while the EWA is not valid quantitatively, the qualitative behavior is similar.

To investigate the validity of the EWA we compare the EWA to the full result for two different assumed Higgs masses above the W pair production threshold. In the left panel of Fig. 3 we show the p_T distributions for the two tagging jets for an assumed Higgs mass of 1 TeV. Only the signal subprocess $ud \to duH$ on the Higgs mass pole is included. Indeed, the distributions for both, transverse and longitudinal W and Z polarizations agree well with the EWA predictions in Eq. (5). Note that for the transverse part even a Higgs mass of 1 TeV shows worse agreement for higher momenta, suggesting a different falloff behavior. For lighter Higgs bosons the agreement becomes gradually worse, as can be seen for $m_H = 180$ GeV in the right panel of Fig. 3. Below the threshold value $m_H = 2m_W$ the EWA assuming incoming on-shell W bosons loses its validity. Nevertheless, the effective W approximation motivates a study of the transverse momenta of the tagging jets to extract information on the polarization of the initial W and Z bosons.

For our actual analysis we use the full amplitude given by Eq. (4). As a first background this includes off-shell W pair production at the same purely electroweak order in perturbation theory. One irreducible background is given by the same initial and final state and with an intermediate Higgs boson, but coupling the Higgs to two gluons at order $\mathcal{O}(\alpha_{ggH}\alpha_s^2\alpha)$. An additional non-Higgs background is W pair production in association with two jets at order $\mathcal{O}(\alpha_s^2\alpha^2)$ [28]. The kinematics of the two tagging jets [26] and the structure of additional central QCD radiation [29] can be used to suppress these backgrounds. In particular through the additional jet activity there exist many ways to reduce the $t\bar{t}+$jets background [28] and we therefore omit it in this first study and limit ourselves to the more dangerous W^+W^- processes on and off the Higgs mass shell. We start by requiring that the W decay leptons ($\ell = e, \mu$) satisfy the staggered cuts

$$|\eta_\ell| < 2.5 \qquad p_{T,\ell} > 20, 10 \text{ GeV} \qquad p_T^{\text{miss}} > 20 \text{ GeV}. \tag{6}$$

The two forward partons forming the tagging jets have to fulfill the standard weak–boson–fusion cuts [27,28]

$$|\eta_j| < 5.0 \qquad p_{T,j} > 25 \text{ GeV} \qquad \Delta\eta_{jj} > 4.2$$
$$m_{jj} > 500 \text{ GeV} \qquad \eta_{j_1} \cdot \eta_{j_2} < 0. \tag{7}$$

Following the definition of longitudinal and transverse W and Z bosons in Eq. (3) we simulate 529 parameter points in the (a_L, a_T) space. Of these 441 are evenly distributed in

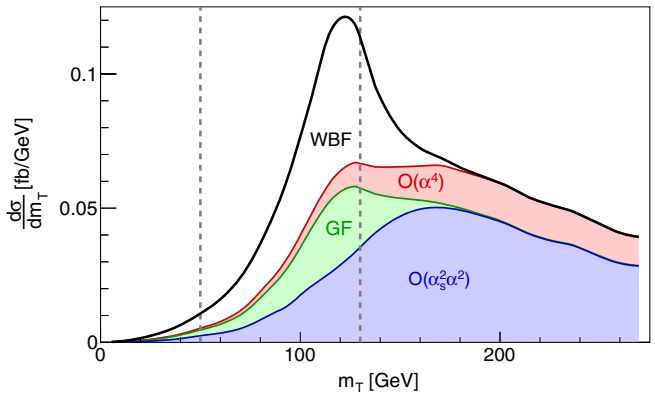

FIG. 4 (color online). Transverse mass distribution for the signal and backgrounds in the standard model. The dashed lines indicate our selection cuts.

TABLE I. Corresponding cross sections for the different subprocesses before and after the m_T cut.

	All	m_T cut
WBF $H \to W^+W^-$	3.15	2.34
Continuum $\mathcal{O}(\alpha^4)$	4.54	0.31
GF $H \to W^+W^-$	1.62	1.13
Continuum $\mathcal{O}(\alpha_s^2\alpha^2)$	11.01	1.17
$S/(S+B)$	0.15	0.47

the range $a_{L/T} \in [-2, 2]$, while 88 increase the sensitivity close to the standard-model value $a_L = a_T = 1$. For each parameter point we generate approximately 10^5 events. In between these points we interpolate cross sections and p-values by Delauny triangulation.

To select events from the Higgs resonance, we use a transverse mass variable m_T, which we define using the approximation $m_{\nu\nu} \approx m_{\ell\ell}$ [28,30]. In Fig. 4 we show the different contributions to the transverse mass distribution. The selection cut

$$50 \text{ GeV} < m_{T,WW} < 130 \text{ GeV} \tag{8}$$

retains 74% of the Higgs resonance events, leading to a signal–to–background ratio around unity. The standard model cross sections before and after this cut for the different processes are given in Table I. For the remainder of this work, we require the transverse on-shell condition of Eq. (8) in addition to the lepton cuts of Eq. (6) and tagging jet cuts of Eq. (7).

IV. RESULTS FOR THE SIMPLE MODEL

Following the discussion in the last section we will focus on Higgs production in weak boson fusion, with a subsequent decay to a leptonic W^+W^- pair. Based on Eq. (3) we define Higgs couplings to transverse and longitudinal W and Z bosons, both contributing to the Higgs signature. In the following we will answer the question which observables will allow us to constrain the two coupling parameters a_L and a_T, both normalized to the standard model value $a_{L,T} = 1$, at the upcoming LHC run.

A. Total rate

The first observable we analyze is the total cross section on the Higgs resonance, measured as the signal strength in the two–jet category both by ATLAS and by CMS [31]. In Fig. 5 we give this cross section after cuts, Eqs. (6)–(8), as a function of a_L and a_T. The curve with a constant cross section is approximately an ellipse in the (a_L, a_T) plane. Close to the standard model the rate is nearly insensitive to the transverse coupling. This reflects the fact that the Higgs boson in the standard model couples predominantly to longitudinal massive gauge bosons. This parameter space region of constant cross section is where additional

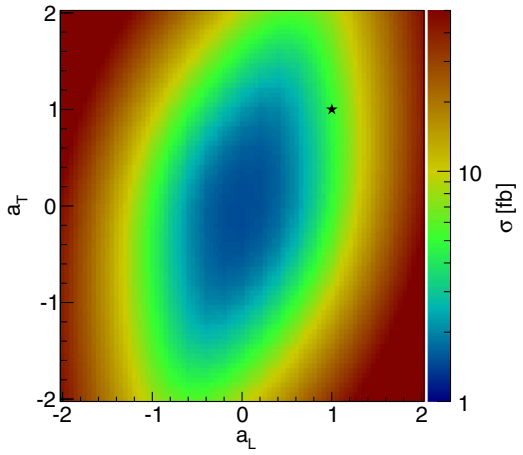

FIG. 5 (color online). Cross sections on the Higgs resonance for various couplings of the Higgs boson to longitudinal and transverse vector bosons. The standard model is marked with a star.

kinematic features are necessary to get more precise information on the individual couplings $a_{L,T}$.

B. Transverse jet momenta

As argued in Sec. III we next focus on the kinematic features of the two tagging jets. Motivated by the effective W approximation we expect the transverse momentum of both jets to be sensitive to the Higgs–gauge coupling structure. In the left panel of Fig. 6 we show distributions of the transverse momentum of the leading jet for the standard model and four additional parameter points, all giving the same cross section. In the right panel we show the average transverse momentum of the leading jet as a function of the location in parameter space. An analysis of the subleading jet shows a similar, but slightly less pronounced behavior.

As shown in Fig. 6, a deviation from the standard model typically leads to a shift to larger transverse momenta of the tagging jets. While the standard model does not mark the (a_L, a_T) point with the minimal average $p_{T,j}$, this minimum is not far away. It is shifted slightly toward larger transverse coupling. The effect of modified couplings on the $p_{T,j}$ distributions is clearly visible, but not huge. Moreover, it is not clear how well these signatures survive hadronization, jet clustering and detector effects.

The individual transverse momenta of the leading jet, $p_{T,j1}$, and that of the subleading jet, $p_{T,j2}$, are not the only potentially relevant observables. We also consider a parametrization in terms of the average transverse momentum and the asymmetry in the transverse momenta between the two jets,

$$\bar{p}_T = \frac{p_{T,j1} + p_{T,j2}}{2} \qquad A_{pT} = \frac{(p_{T,j1} - p_{T,j2})}{(p_{T,j1} + p_{T,j2})}. \tag{9}$$

In particular, we expect the asymmetry to be robust under systematic uncertainties that affect the p_T measurements of both jets alike.

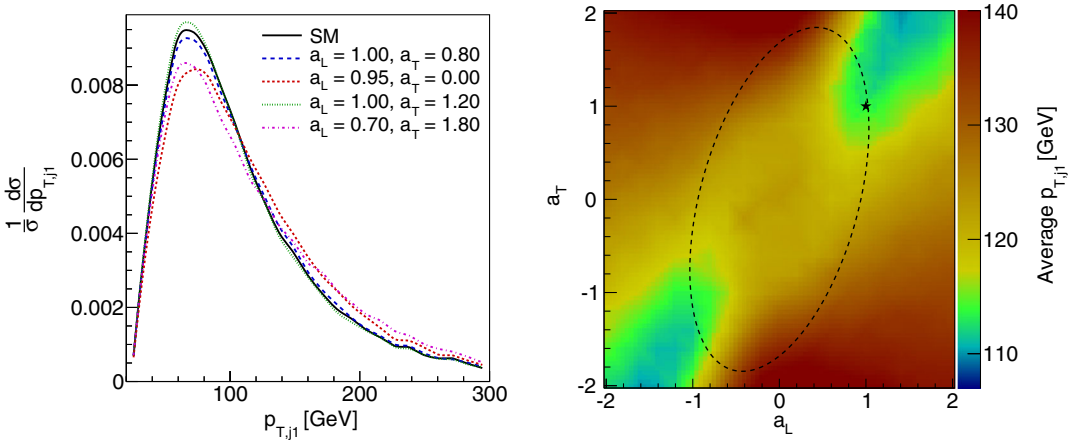

FIG. 6 (color online). Left: normalized leading $p_{T,j}$ distribution for the a few example points, all giving a standard model rate. Right: average leading $p_{T,j}$ as a function of the couplings. The ellipse indicates a constant rate following Fig. 5.

We find that $\bar{p}_T$ behaves very similar to the transverse momentum of the leading jet: deviations from the standard model tend to shift its distribution to larger values. In the left panel of Fig. 7 we give distributions of A_{pT} for the same example points as before. A modification of the Higgs–gauge couplings slightly favors lower values of A_{pT}. So by moving away from the standard model in parameter space, both jets gain transverse momentum, and the subleading jet increases by a larger factor than the leading jet.

We also investigate the vectorial sum and difference of the two transverse jet momenta. Unlike the quantities discussed above, these observables depend on the angular correlation between the two jets. The distribution of the vectorial sum is shown in the right panel of Fig. 7. For $a_L > a_T$, this quantity is shifted to larger values, while a more transverse Higgs–gauge coupling structure favors lower scales. The vectorial difference changes less strongly with the parameters and shows the opposite behavior: a shift to more longitudinal couplings reduces the observable slightly, while a more transverse coupling structure increases this difference a little.

C. Azimuthal angle

In addition to the transverse momenta we can also study angular correlations between the two tagging jets. In the left panel of Fig. 8 we show the distribution of $\Delta\phi_{jj}$ [21] for the same parameter points as before. It turns out that Higgs–gauge couplings different from the standard model leave a clear signature. Unlike for the transverse momenta, the standard model does not lead to a particular distribution: with $a_L > a_T$, the jets tend to be more collinear in the transverse plane. Conversely, a small relative increase of the transverse coupling favors back-to-back geometries.

In order to quantify this effect in a way that minimizes systematic uncertainties, we define the asymmetry [20]

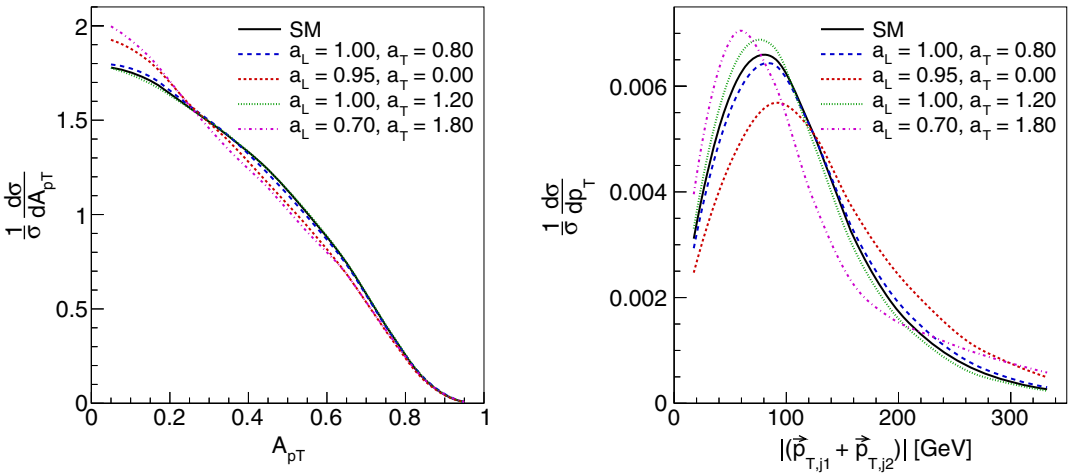

FIG. 7 (color online). Left: normalized distribution of the asymmetry A_{pT} between the transverse momenta of the two jets, as defined in Eq. (9), for a few example points, all giving a standard model rate. Right: normalized distribution of the vectorial sum of the transverse momenta of the jets for the same example points.

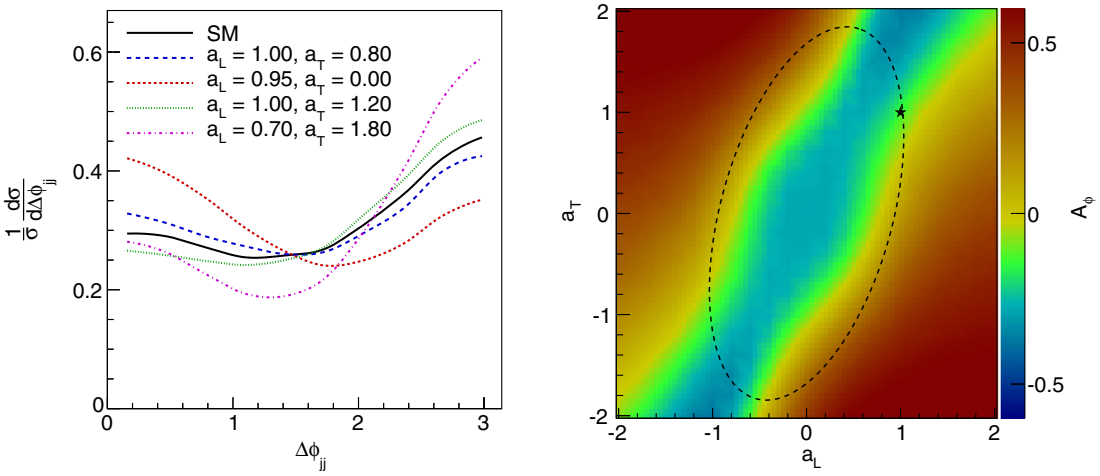

FIG. 8 (color online). Left: normalized $\Delta\phi_{jj}$ distribution for the a few example points, all giving a standard model rate. Right: the asymmetry A_ϕ as defined in Eq. (10) as a function of the couplings. The ellipse indicates a constant rate following Fig. 5.

$$A_\phi = \frac{\sigma(\Delta\phi_{jj} < \frac{\pi}{2}) - \sigma(\Delta\phi_{jj} > \frac{\pi}{2})}{\sigma(\Delta\phi_{jj} < \frac{\pi}{2}) + \sigma(\Delta\phi_{jj} > \frac{\pi}{2})}. \tag{10}$$

We give the distribution of A_ϕ over the (a_L, a_T) parameter space in the right panel of Fig. 8. It shows the same behavior as expected from an analysis of the full $\Delta\phi_{jj}$ distributions. Deviations from the SM Higgs–gauge coupling are easily visible in A_ϕ.

The discrimination power of the p_T distributions and of the angular correlation between the tagging jets is of similar constraining power, but in an orthogonal direction to the information encoded in the cross section. A combination of rate measurements with kinematic observables will therefore efficiently restrict the parameter space consistent with data.

We can also test whether the tagging jet properties are correlated with the polarization of the final gauge bosons [15]. We find that for the pure Higgs signal they are entirely uncorrelated, reflecting the scalar nature of the Higgs boson where the decay mode knows nothing about its production. Including the backgrounds, a correlation emerges, caused by the fact that final-state longitudinal WW pairs are more likely to stem from a signal events, while transverse bosons have a larger probability to come from a background interaction.

D. Other observables

So far, we have restricted our analysis to observables describing the jet kinematics in the transverse plane, and found them to be sensitive to the Higgs–gauge coupling structure. We have also analyzed the distribution of quantities that are (mostly) sensitive to the longitudinal jet momentum. These include the jet energies, the invariant mass between the two jets, as well as their separation in pseudorapidity. We find that all of these observables are much less sensitive to the structure of the Higgs–gauge sector than the purely transverse quantities discussed above. This does not come as a surprise: the longitudinal momentum of the final-state quarks in the WBF topology is dictated by the incoming quarks, which at the LHC set a much larger scale than that describing the hard $WW \to H$ process. Since including these variables does not improve the significance of our findings, we limit our analysis to the transverse jet momenta and the angular correlation between the jets in the transverse plane.

E. Combination

In a next step, we estimate the sensitivity in the (a_L, a_T) plane when measuring these kinematical features. This will give us the parameter space which can be probed during the upcoming LHC run. We generate a number of toy data samples based on the standard model, representing an integrated luminosity of 300 fb^{-1}. Each of these toy data samples is compared to the samples based on our simple model. We determine the significance of deviations in the Higgs cross section and the asymmetry A_ϕ by calculating the probability density functions of these quantities for each parameter point of our simple model. For the other kinematic observables discussed above, we measure the significance of deviations by performing χ^2 tests on the normalized distributions. From these tests we extract the median p-value. If it is below 0.05, the parameter point (a_L, a_T) in question is expected to be excluded at 95% CL in the absence of a signal. The results from certain sets of observables are statistically independent and can be combined correspondingly.

In Table II we give the limits on the parameters a_L and a_T obtained using different combinations of observables. In general, observables including the angular correlation between the jets give stronger constraints than those based only on transverse momenta. However, an analysis based only on the $\Delta\phi_{jj}$ distribution or only on the asymmetry A_ϕ

TABLE II. Limits on $a_{L,T} \in [0, 2]$ in the absence of a signal based on different observables. The limits are given at 95% CL assuming 300 fb^{-1}. For the limit on a_L, a_T is allowed to float freely, and vice versa.

Observables	Limit on a_L	Limit on a_T
σ	($\leq$1.07)	($\leq$1.97)
σ, $p_{T,j1}$	(0.76–1.08)	(0.25–1.79)
σ, $p_{T,j1}$, $p_{T,j2}$	(0.82–1.08)	(0.56–1.68)
σ, $\bar{p}_T$	(0.79–1.07)	(0.41–1.73)
σ, A_{pT}	(0.65–1.08)	($\leq$1.86)
σ, $\bar{p}_T$, A_{pT}	(0.78–1.09)	(0.39–1.73)
σ, $\Delta\phi_{jj}$	(0.49–0.54) and (0.95–1.06)	(0.83–1.17) and (1.89–1.94)
σ, A_ϕ	(0.52–0.64) and (0.94–1.06)	(0.82–1.15) and (1.77–2.00)
σ, $\lvert(\vec{p}_{T,j1} + \vec{p}_{T,j1})\rvert$	(0.93–1.06)	(0.66–1.28)
σ, $\lvert(\vec{p}_{T,j1} - \vec{p}_{T,j1})\rvert$	($\leq$0.61) and (0.85–1.08)	($\leq$1.96)
σ, $p_{T,j1}$, $p_{T,j2}$, $\Delta\phi_{jj}$	(0.92–1.08)	(0.82–1.19)
σ, $p_{T,j1}$, $p_{T,j2}$, A_ϕ	(0.92–1.08)	(0.80–1.18)

leads to a binary ambiguity: there is a blind spot in the parameter space around the parameters $a_L \approx 0.6$, $a_T \approx 1.8$. This region shows the same rate and angular correlation between the jets as the standard model. Including the transverse jet momentum in the analysis removes this ambiguity. All in all, a combination of the cross section with the transverse momenta of the leading and subleading jet as well as the asymmetry A_ϕ yields the strongest constraints on the parameters of our simple model.

In Fig. 9 we show the expected exclusion regions for these observables. With an integrated luminosity of 300 fb^{-1} they can be used to exclude most of the (a_L, a_T) plane. At least on parton level and disregarding systematic uncertainties, the coupling factor a_L should be measurable at $\mathcal{O}(10\%)$, while the transverse coupling should be measurable at $\mathcal{O}(20\%)$. The mirrored solution with $a_L \approx -1$, $a_T \approx -1$ cannot be excluded in this analysis. However, the $H \to \gamma\gamma$ decay, mediated by a top loop and a W loop, is easily sensitive to this sign change.

While we neglect theoretical and systematic uncertainties, we also show the results of the same analysis after including a hypothetical uncertainty of $\pm 10\%$ on the Higgs production and decay rate. At this level of analysis it is simply not clear how large the different uncertainties are. This will largely depend on the central jet veto or alternative analysis [29] and the associated theoretical uncertainties.

V. CHOICE OF REFERENCE FRAME

In the setup described above we define the polarization of the virtual gauge bosons in the Higgs rest frame. This leads us to results fully consistent with the expectations from the effective W approximation. However, while the definition of

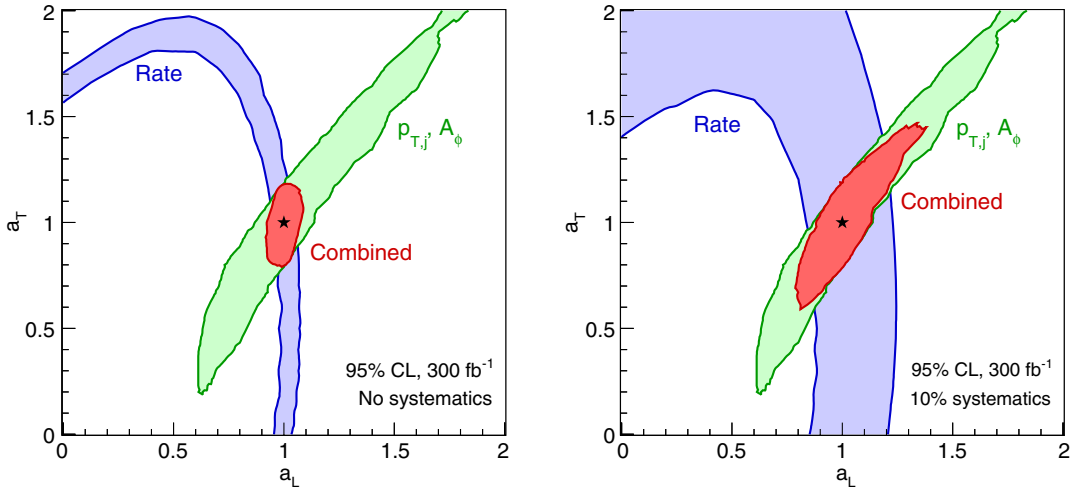

FIG. 9 (color online). Expected exclusion regions at 95% CL after 300 fb^{-1} of data in the absence of a signal. Note that these are results calculated at parton level and not including any systematic uncertainties. In the right panel we show the same result including an additional 10% uncertainty on the Higgs production and decay rate.

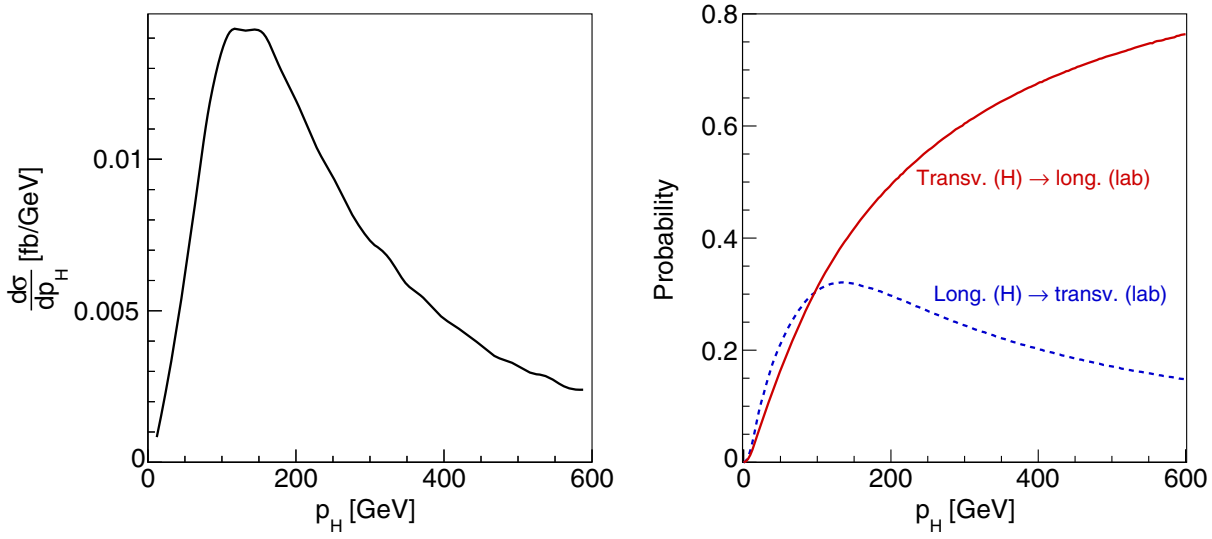

FIG. 10 (color online). Left: distribution of the Higgs momentum in the SM after our selection cuts. Right: probabilities for a change in polarization when going from the Higgs rest frame to the laboratory frame as a function of the Higgs momentum.

polarizations requires a reference frame, in the absence of a V rest frame there remains a choice of frames. In this section we will briefly review the effect of a different choice.

To link the different reference frames we have to understand how polarizations change during boosts. The tagging jet distributions probe the HVV vertex in the weak–boson–fusion production of an on-shell Higgs boson. Here, we will for simplicity consider the Higgs decay to an on-shell and an off-shell V boson instead. The polarization of the V bosons in the Higgs rest frame changes when we apply a boost into another frame with a finite Higgs momentum $\vec{p}_H$ in that new frame. The probability of a transverse boson becoming longitudinal or vice versa depends on the size of the boost as well as the angle between the boost direction and the V momenta, where in our brief discussion we average over the relative angle. In the left panel of Fig. 10 we give the distribution of the Higgs momentum for our reference process in the laboratory frame. It ranges around 100–300 GeV. In the rest frame of the two colliding partons the typical Higgs momentum is slightly reduced.

Given this momentum range we calculate the probability for a transverse V in the Higgs rest frame to become longitudinal after the boost, and vice versa. We give the results in the right panel of Fig. 10. For Higgs momenta around 200 GeV, corresponding to a $\gamma \sim 2$, the probability for a change in polarization reaches $\mathcal{O}(50\%)$; the polarizations are essentially randomized. Any clear effect in the Higgs rest frame is washed out in any frame with such a relative boost.

In the following we will show that the VV rest frame or equivalently the Higgs rest frame is well suited to analyze polarization effects in VV scattering. Moreover, we will see that a definition in this frame also nicely compares with an approach based on higher-dimensional operators. Defining the polarizations in the laboratory frame or the rest frame of the two colliding partons therefore leads to qualitatively similar, but much less pronounced findings.

VI. EFFECTIVE FIELD THEORY

Complementing our simple model we can parametrize structural deviations from the standard model in terms of higher-dimensional operators. This has the advantage of being manifestly Lorentz invariant, so it can serve as a check of our assumption that the definition of the transverse vs longitudinal reference frame at finite energies has little impact on our physics results.

Without adding new operator structures to the standard model Lagrangian $\mathcal{L}_{\rm SM}$ we can allow for changes in the Higgs coupling strength to two vector bosons. For more drastic changes, in particular affecting longitudinal and transverse gauge bosons differently and hence leading to different tagging jet properties, we invoke new operator structures. The question is how the obvious physical description of gauge boson polarizations used in the previous sections can be phrased in terms of such higher dimensional operators,

$$\mathcal{L}_{\rm D6} = \mathcal{L}_{\rm SM} + \sum_i \frac{c_i}{\Lambda^2} \mathcal{O}_i. \tag{11}$$

As an example we will study two electroweak operators including the usual Higgs doublet ϕ,

$$\mathcal{O}_{\phi,2} = \frac{1}{2} \partial_\mu (\phi^\dagger \phi) \partial^\mu (\phi^\dagger \phi) \quad \text{and}$$
$$\mathcal{O}_W = (D_\mu \phi)^\dagger \hat{W}^{\mu\nu} (D_\nu \phi), \tag{12}$$

following the conventions discussed in Refs. [6,32,33]. For instance, these operators arise in strongly interacting Higgs sectors [34,35], including little Higgs [36] and holographic Higgs [37] models.

First, the operator $\mathcal{O}_{\phi,2}$ generates a new contribution to the Higgs kinetic term $\partial_\mu H \partial^\mu H$. A field redefinition $H \to H/\sqrt{1+c_{\phi 2} v^2/\Lambda^2}$ restores (most of) the canonical normalization of the kinetic term [30,34], but also introduces a form factor for every Higgs vertex. Following the definition in Eq. (3), the HWW interaction is modified by the universal factor

$$a_L = a_T = 1 - \frac{c_{\phi 2}}{2}\frac{v^2}{\Lambda^2}, \tag{13}$$

that does not depend on the momenta. It is therefore in one-to-one correspondence with the $a_L = a_T$ case in our simple model. Because $\mathcal{O}_{\phi,2}$ only shifts Higgs interactions universally it is hardly constrained by electroweak precision measurements and the measurement of triple gauge vertices.

For the operator $\mathcal{O}_W$ the situation is more interesting. It modifies the interaction between the weak gauge bosons and the Higgs boson, but there is no term of order ϕ^3 or higher contributing to the Higgs–Goldstone couplings. At large energies it therefore shifts the transverse Higgs–gauge coupling, but not its longitudinal counterpart. While the Higgs resonance hardly constitutes a high-energy limit, we expect the effect of $\mathcal{O}_W$ on the longitudinal coupling a_L to be suppressed as compared to a_T.

In unitary gauge the operator $\mathcal{O}_W$ yields two types of corrections to the HWW vertex,

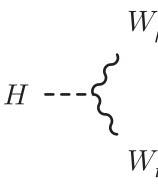

$$= igm_W \Big[\underbrace{g_{\mu\nu} - g_{\mu\nu}\frac{c_W}{2\Lambda^2}\left((p^H p^+) + (p^H p^-)\right)}_{a_{L,T}^{(1)}} + \underbrace{\frac{c_W}{2\Lambda^2}\left(p_\mu^H p_\nu^+ + p_\mu^- p_\nu^H\right)}_{a_{L,T}^{(2)}} \Big], \tag{14}$$

where $p_\mu^\pm$ and p_μ^H are the incoming momenta of the $W^\pm$ and the H, respectively. The first two terms of Eq. (14) correspond to the standard model vertex and an unchanged Lorentz structure with a higher-dimensional coupling strength modification. For an on-shell Higgs these two terms give us

$$a_L^{(1)} = a_T^{(1)} = 1 + \frac{c_W}{2\Lambda^2} m_H^2. \tag{15}$$

The last term in Eq. (14) features contractions of the type $(p^H \varepsilon^\pm)$, where $\varepsilon^\pm$ are the polarization vectors of the $W^\pm$ bosons. In the Higgs rest frame, this terms vanishes for transverse gauge bosons, but its contribution to the longitudinal coupling does not. Unlike in our simple model, this factor is a function of the W momenta,

$$a_T^{(2)} = 0 \qquad a_L^{(2)} = \frac{c_W}{\Lambda^2} F(p^+, p^-). \tag{16}$$

The operator $\mathcal{O}_W$ does not only affect Higgs physics, but clearly also contributes to the ZWW and WWW interactions. Still, there are no strong constraints from electroweak precision measurements of the oblique parameters S, T and U. This is because the loop contributions from this operator can be balanced by other operators, making this operator a so-called "blind direction" [38]. The strongest limits on c_W hence stem from measurements of triple gauge boson vertices at the LHC [39].

We can compare the effects of both approaches on our leading kinematic distributions. Let us first separately consider the modification of the HWW vertex by the first term and second term of Eq. (14). In both cases we choose $c_{\phi,2}/\Lambda^2 = \pm 10/\text{TeV}^2$, which is slightly outside current exclusion limits [39], in order to make the effect of this operator more visible. In these two setups we compute cross sections as well as p_T and $\Delta\phi_{jj}$ distributions. The results are shown in Fig. 11 as the red and blue solid lines.

Considering only the first term of Eq. (14), i.e. shifting the standard model coupling strength, we find that the cross section noticeably increases with positive c_W and decreases with negative c_W in line with our expectation from Eq. (15). We can now compare to our simple model. The dashed lines in the left panels of Fig. 11 correspond to the results of our simple model with parameters chosen according to Eq. (15). The agreement is very good, as one would expect, because the shift in $a_{L,T}$ is momentum-independent for an on-shell Higgs. The only differences can arise from the (small) off-shell Higgs contributions that survive the cuts we have made.

The second term of Eq. (14) introduces new Lorentz structures. It not only modifies the rate, but also changes the kinematic features. In particular, the couplings $a_{L,T}$ that were constant in our simple model now depend on the momenta. Positive values of c_W now lead to a significantly reduced cross section, reflecting the relative sign between the two dimension-6 contributions. They also slightly

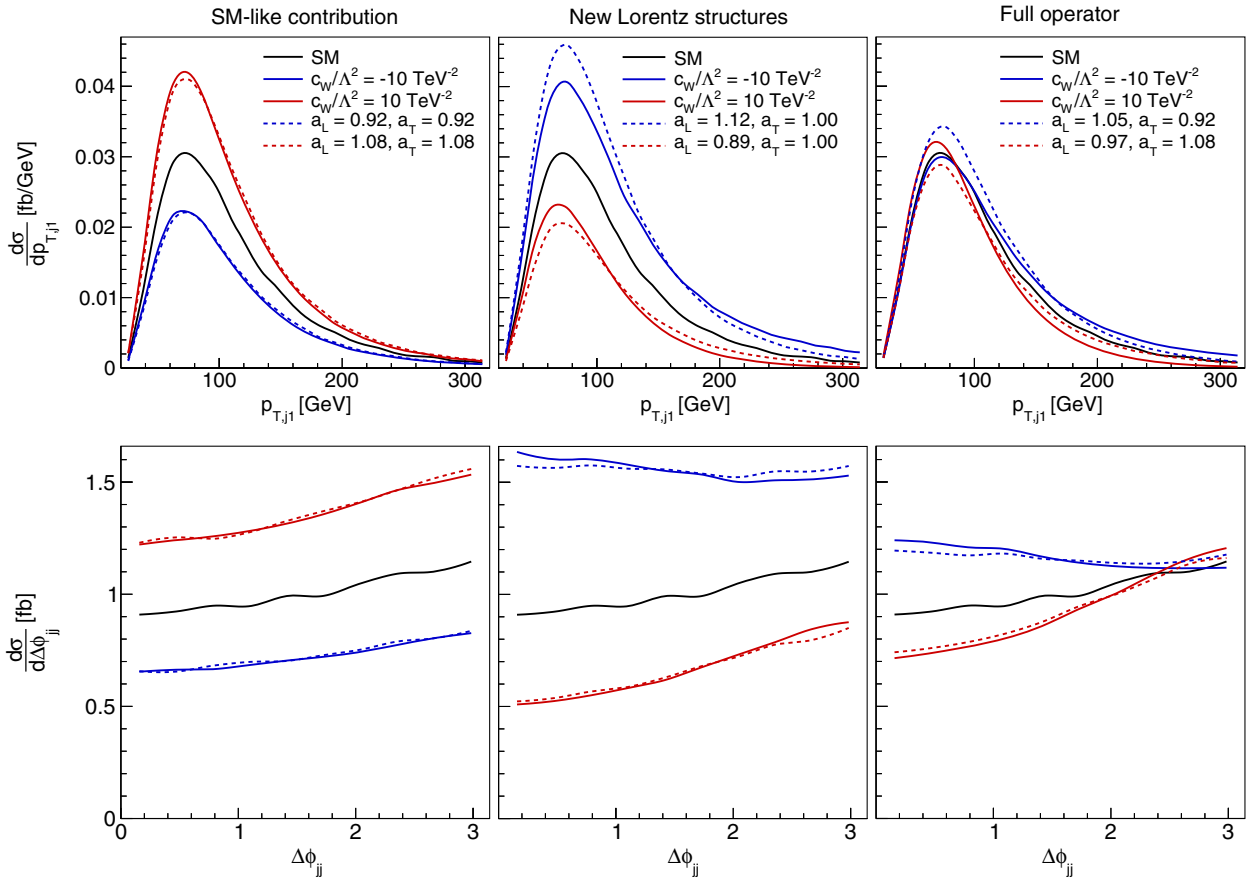

FIG. 11 (color online). Effects of $\mathcal{O}_W$ on kinematic distributions and the corresponding results from our simple model. For the first we separate the first terms (left panels) and second term (middle panels) as defined in Eq. (14). The right panels show the effect of the full operators.

soften the tagging jets and induce a preference for back-to-back configurations of the two tagging jets. Conversely, negative c_W increase the rate, lead to harder tagging jets, and favor aligned tagging jets.

To compare with our simple model we fit a constant a_L ($a_T = 1$ as argued above). For instance, for $c_W/\Lambda^2 = 10/\text{TeV}^2$ we find that a constant longitudinal coupling $a_L^{(2)} = 0.89$ corresponding to $F(p^+, p^-) = -(105\ \text{GeV})^2$ yields good agreement in the cross section and the angular correlation between $\mathcal{O}_W$ and our simple model. This can be seen in the bottom middle panel of Fig. 11. However, the transverse momentum of the leading tagging jet, shown in the top right panel of Fig. 11, indicates substantial deviations. For positive c_W the tagging jets in the dimension-6 approach are softer while for negative c_W they are harder than in our simple model. This reflects the fact that a constant value of $F(p^+, p^-)$ entering $a_L^{(2)}$ does not account for the momentum dependence of $\mathcal{O}_W$.

Ignoring the momentum dependence, the preferred effective value of $F(p^+, p^-)$ is worth a brief discussion. It describes a contribution to the longitudinal coupling that is antiproportional to the effect of the first term in Eq. (14). After combining, the two modifications of the longitudinal coupling nearly cancel for $c_W/\Lambda^2 = 10/\text{TeV}^2$, while the transverse coupling is unaffected by the second modification:

$$a_L^{(1)} + a_L^{(2)} = 1 + \frac{c_W}{\Lambda^2}\left(\frac{1}{2}m_H^2 - (105\ \text{GeV})^2\right) = 0.97,$$
$$a_T^{(1)} + a_T^{(2)} = 1 + \frac{c_W}{2\Lambda^2}m_H^2 = 1.08. \quad (17)$$

This means that $\mathcal{O}_W$ primarily affects the transverse Higgs–gauge interactions, as expected from the equivalence theorem.

A final comparison between the full operator $\mathcal{O}_W$ and the corresponding simple model as shown in the right panels of Fig. 11 supports these observations. The large effects on the cross sections from the individual two terms, which correspond to a large modification of the longitudinal coupling, partly cancel. We are left with a modest decrease of the rate for positive c_W and an increase for negative c_W. The kinematical distributions follow exactly the same pattern as for the second term only. The simple model, where the equivalent coupling a_L is now close to one, predicts rates and $\Delta\phi_{jj}$ distributions in good agreement

with the dimension-6 results. The discrepancy in the jet p_T distribution reflecting the missing momentum dependence remains as well.

All in all we find that while not all details can be directly linked to higher-dimensional operators, our simple model gives a good description of the qualitative features in terms of the intuitive gauge boson polarizations.

VII. CONCLUSIONS

Based on the Goldstone equivalence theorem, one can argue that deviations from the standard model Higgs couplings to transverse and longitudinal gauge bosons could have a very distinctive physics origin. The longitudinal gauge bosons are inherently connected to features of the Higgs sector, whereas those of the transverse ones test the nature of the original gauge bosons.

While such tests of the Higgs–gauge sector are theoretically and experimentally well established for the high-energy regime, we propose to extend this approach to the Higgs resonance. Experimentally, this strategy has the benefit of significantly higher rates, so we can try to search for deviations from the standard model in the bulk of the $VV \to VV$ cross section rather than in its tails.

On the theory side, the separation of gauge boson polarizations away from the high-energy limit requires some care. In particular it suffers from the fact that to perform this separation one has to explicitly break Lorentz invariance to define polarizations. Independent of this issue, the observables we investigate can be viewed as a first step toward testing such physics and can more generally be useful in probing the structure of the Higgs–gauge sector. We have demonstrated this in a comparison with a fully Lorentz-invariant model based on effective field theory. In particular, we have shown that independent couplings of longitudinal and transverse gauge bosons to the Higgs can be generated in a model described by dimension-six electroweak operators.

We complement the information from the total rate at the Higgs resonance with the kinematics of the tagging jets. Both their transverse momenta and their angular correlation provide valuable information on the structure of the HVV coupling, parametrized in terms of the longitudinal and transverse gauge boson polarizations. The constraints from the kinematical distributions are orthogonal to the constraints from the cross section. When it comes to numbers, systematic effects become relevant. In this first study we have limited ourselves to a parton-level analysis of the dominant signal and background processes, omitting theoretical and systematic uncertainties. Combining the cross section and tagging jet observables, longitudinal and transverse gauge boson couplings to the Higgs can be individually probed at the $\mathcal{O}(20\%)$ level using 300 fb^{-1} of integrated luminosity at 13 TeV.

[1] P. W. Higgs, Phys. Lett. **12**, 132 (1964); **13**, 508 (1964); Phys. Rev. **145**, 1156 (1966); F. Englert and R. Brout, Phys. Rev. Lett. **13**, 321 (1964); G. S. Guralnik, C. R. Hagen, and T. W. Kibble, Phys. Rev. Lett. **13**, 585 (1964).

[2] G. Aad *et al.* (ATLAS Collaboration), Phys. Lett. B **716**, 1 (2012); S. Chatrchyan *et al.* (CMS Collaboration), Phys. Lett. B **716**, 30 (2012).

[3] See e.g. for a review D. E. Morrissey, T. Plehn, and T. M. P. Tait, Phys. Rep. **515**, 1 (2012).

[4] See e.g. M. Shaposhnikov and C. Wetterich, Phys. Lett. B **683**, 196 (2010); M. Holthausen, K. S. Lim, and M. Lindner, J. High Energy Phys. 02 (2012) 037; A. Hebecker, A. K. Knochel, and T. Weigand, Nucl. Phys. **B874**, 1 (2013); D. Buttazzo, G. Degrassi, P. P. Giardino, G. F. Giudice, F. Sala, A. Salvio, and A. Strumia, J. High Energy Phys. 12 (2013) 089.

[5] C. H. Llewellyn Smith, Phys. Lett. **46B**, 233 (1973); D. A. Dicus and V. S. Mathur, Phys. Rev. D **7**, 3111 (1973); B. W. Lee, C. Quigg, and H. B. Thacker, Phys. Rev. D **16**, 1519 (1977); M. J. G. Veltman, Acta Phys. Pol. B **8**, 475 (1977).

[6] For an overview see e.g., I. Brivio *et al.*, S. Willenbrock and C. Zhang, C. Englert, A. Freitas, M. Mühlleitner, T. Plehn, M. Rauch, M. Spira, and K. Walz (to be published).

[7] M. S. Chanowitz and M. K. Gaillard, Nucl. Phys. **B261**, 379 (1985).

[8] M. Suzuki, Phys. Rev. D **37**, 210 (1988); A. G. Cohen, H. Georgi, and E. H. Simmons, Phys. Rev. D **38**, 405 (1988); A. Hasenfratz and P. Hasenfratz, Phys. Lett. B **297**, 166 (1992).

[9] Z. Komargodski, J. High Energy Phys. 02 (2011) 019.

[10] N. Seiberg, Nucl. Phys. **B435**, 129 (1995).

[11] K. Cheung, C.-W. Chiang, and T.-C. Yuan, Phys. Rev. D **78**, 051701 (2008); H.-J. He, Y.-P. Kuang, C. P. Yuan, and B. Zhang, Phys. Lett. B **554**, 64 (2003); B. Zhang, Y.-P. Kuang, H.-J. He, and C. P. Yuan, Phys. Rev. D **67**, 114024 (2003).

[12] J. Bagger, S. Dawson, and G. Valencia, Nucl. Phys. **B399**, 364 (1993); J. Bagger, V. D. Barger, K.-m. Cheung, J. F. Gunion, T. Han, G. A. Ladinsky, R. Rosenfeld, and C. P. Yuan, Phys. Rev. D **49**, 1246 (1994); J. Bagger, V. D. Barger, K.-m. Cheung, J. F. Gunion, T. Han, G. A. Ladinsky, R. Rosenfeld, and C.-P. Yuan, Phys. Rev. D **52**, 3878 (1995).

[13] J. M. Butterworth, B. E. Cox, and J. R. Forshaw, Phys. Rev. D **65**, 096014 (2002).

[14] A. Ballestrero, G. Bevilacqua, D. B. Franzosi, and E. Maina, J. High Energy Phys. 11 (2009) 126; A. Ballestrero, D. B. Franzosi, and E. Maina, J. High Energy Phys. 06 (2011) 013; A. Ballestrero, D. B. Franzosi, L. Oggero, and E. Maina, J. High Energy Phys. 03 (2012) 031; A. Ballestrero, D. B. Franzosi, and E. Maina, J. High Energy Phys. 05 (2012) 083.

[15] T. Han, D. Krohn, L.-T. Wang, and W. Zhu, J. High Energy Phys. 03 (2010) 082.
[16] J. Alwall, M. Herquet, F. Maltoni, O. Mattelaer, and T. Stelzer, J. High Energy Phys. 06 (2011) 128.
[17] G. Aad *et al.* (ATLAS Collaboration), J. High Energy Phys. 04 (2014) 031.
[18] A. Djouadi, J. Kalinowski, and M. Spira, Comput. Phys. Commun. **108**, 56 (1998).
[19] V. D. Barger, G. Bhattacharya, T. Han, and B. A. Kniehl, Phys. Rev. D **43**, 779 (1991); M. Dittmar and H. K. Dreiner, Phys. Rev. D **55**, 167 (1997).
[20] T. Plehn, D. L. Rainwater, and D. Zeppenfeld, Phys. Rev. Lett. **88**, 051801 (2002).
[21] O. J. P. Eboli and D. Zeppenfeld, Phys. Lett. B **495**, 147 (2000); T. Plehn, D. L. Rainwater, and D. Zeppenfeld, Phys. Rev. Lett. **88**, 051801 (2002); V. Hankele, G. Klamke, D. Zeppenfeld, and T. Figy, Phys. Rev. D **74**, 095001 (2006); C. Ruwiedel, N. Wermes, and M. Schumacher, Eur. Phys. J. C **51**, 385 (2007); K. Hagiwara, Q. Li, and K. Mawatari, J. High Energy Phys. 07 (2009) 101; A. Djouadi, R. M. Godbole, B. Mellado, and K. Mohan, Phys. Lett. B **723**, 307 (2013).
[22] C. Englert, D. Goncalves-Netto, K. Mawatari, and T. Plehn, J. High Energy Phys. 01 (2013) 148.
[23] V. Del Duca, W. Kilgore, C. Oleari, C. Schmidt, and D. Zeppenfeld, Nucl. Phys. **B616**, 367 (2001); J. R. Andersen, K. Arnold, and D. Zeppenfeld, J. High Energy Phys. 06 (2010) 091; F. Campanario, M. Kubocz, and D. Zeppenfeld, Phys. Rev. D **84**, 095025 (2011); C. Englert, D. Goncalves, G. Nail, and M. Spannowsky, Phys. Rev. D **88**, 013016 (2013); F. Campanario and M. Kubocz, Phys. Rev. D **88**, 054021 (2013).
[24] M. R. Buckley and M. J. Ramsey-Musolf, J. High Energy Phys. 09 (2011) 094; K. Hagiwara and S. Mukhopadhyay, J. High Energy Phys. 05 (2013) 019; M. R. Buckley, T. Plehn, and M. J. Ramsey-Musolf (unpublished).
[25] S. Dawson, Nucl. Phys. **B249**, 42 (1985); G. L. Kane, W. W. Repko, and W. B. Rolnick, Phys. Lett. **148B**, 367 (1984); see also P. Borel, R. Franceschini, R. Rattazzi, and A. Wulzer, J. High Energy Phys. 06 (2012) 122.
[26] R. Kleiss and W. J. Stirling, Phys. Lett. B **200**, 193 (1988); U. Baur and E. W. N. Glover, Phys. Lett. B **252**, 683 (1990); V. D. Barger, K. Cheung, T. Han, J. Ohnemus, and D. Zeppenfeld, Phys. Rev. D **44**, 1426 (1991).
[27] D. L. Rainwater, D. Zeppenfeld, and K. Hagiwara, Phys. Rev. D **59**, 014037 (1998); T. Plehn, D. L. Rainwater, and D. Zeppenfeld, Phys. Rev. D **61**, 093005 (2000).
[28] D. L. Rainwater and D. Zeppenfeld, Phys. Rev. D **60**, 113004 (1999); **61**, 099901(E) (2000); N. Kauer, T. Plehn, D. L. Rainwater, and D. Zeppenfeld, Phys. Lett. B **503**, 113 (2001).
[29] V. D. Barger, R. J. N. Phillips, and D. Zeppenfeld, Phys. Lett. B **346**, 106 (1995); D. L. Rainwater, R. Szalapski, and D. Zeppenfeld, Phys. Rev. D **54**, 6680 (1996); V. Del Duca, G. Klämke, M. L. Mangano, M. Moretti, F. Piccinini, R. Pittau, A. D. Polosa, and D. Zeppenfeld, J. High Energy Phys. 10 (2006) 016; C. Bernaciak, M. S. A. Buschmann, A. Butter, and T. Plehn, Phys. Rev. D **87**, 073014 (2013); C. Bernaciak, B. Mellado, T. Plehn, X. Ruan, and P. Schichtel (unpublished).
[30] For pedagogical introductions see e.g., M. Spira and P. M. Zerwas, Lect. Notes Phys. **512**, 161 (1998); A. Djouadi, Phys. Rep. **457**, 1 (2008); T. Plehn, Lect. Notes Phys. **844**, 1 (2012).
[31] G. Aad *et al.* (ATLAS Collaboration), Phys. Lett. B **726**, 88 (2013); S. Chatrchyan *et al.* (CMS Collaboration), J. High Energy Phys. 01 (2014) 096.
[32] K. Hagiwara, S. Ishihara, R. Szalapski, and D. Zeppenfeld, Phys. Rev. D **48**, 2182 (1993).
[33] W. Buchmüller and D. Wyler, Nucl. Phys. **B268** (1986) 621; B. Grzadkowski, M. Iskrzynski, M. Misiak, and J. Rosiek, J. High Energy Phys. 10 (2010) 085.
[34] G. F. Giudice, C. Grojean, A. Pomarol, and R. Rattazzi, J. High Energy Phys. 06 (2007) 045.
[35] D. B. Kaplan, H. Georgi, and S. Dimopoulos, Phys. Lett. **136B**, 187 (1984).
[36] N. Arkani-Hamed, A. G. Cohen, and H. Georgi, Phys. Lett. B **513**, 232 (2001); for a useful review see e.g., M. Schmaltz and D. Tucker-Smith, Annu. Rev. Nucl. Part. Sci. **55**, 229 (2005).
[37] R. Contino, Y. Nomura, and A. Pomarol, Nucl. Phys. **B671**, 148 (2003); K. Agashe, R. Contino, and A. Pomarol, Nucl. Phys. **B719** (2005) 165.
[38] A. De Rujula, M. B. Gavela, P. Hernandez, and E. Masso, Nucl. Phys. **B384**, 3 (1992).
[39] T. Corbett, O. J. P. Eboli, J. Gonzalez-Fraile, and M. C. Gonzalez-Garcia, Phys. Rev. D **87**, 015022 (2013).